RSC Advances

PAPER

View Article Online
View Journal | View Issue

Cite this: *RSC Adv.*, 2017, **7**, 20057

Custom designed $ZnMn_2O_4$/nitrogen doped graphene composite anode validated for sodium ion battery application†

B. Chandra Sekhar, P. Packiyalakshmi and N. Kalaiselvi *

For the first time, pH control driven synthesised $ZnMn_2O_4$ nanoparticles embedded in nitrogen doped graphene sheets (ZMO/NG) have been validated as a sodium ion battery anode that exhibits superior electrochemical performance than a pristine $ZnMn_2O_4$ anode. Sodium-ion chemistry, known for its sustainable and economically viable storage solution providing strategy is gaining paramount importance especially when supported with eco-benign and abundantly available metal(s) based electrode assembly. In this regard, a $ZnMn_2O_4$/NG anode exhibits a stable and appreciable capacity of 170 mA h g^{-1} up to 1000 cycles at 100 mA g^{-1} and an excellent rate capability up to 10 A g^{-1}. The currently observed superior electrochemical performance of the title anode may be ascribed to the synergistic effect of presence of $ZnMn_2O_4$ nanoparticles decorated with the sheets of nitrogen doped graphene in a desirable manner so as to reap the advantages of nitrogen doped graphene in terms of enhanced electrode conductivity, maintenance of structural integrity upon cycling and the effective accommodation of volume changes during charging and discharging. The $ZnMn_2O_4$/nitrogen doped graphene composite anode of the present study finds its place as a better performing SIB anode for extended cycles and excellent rate capability applications.

Received 23rd February 2017
Accepted 30th March 2017

DOI: 10.1039/c7ra02289a

rsc.li/rsc-advances

1. Introduction

Lithium-ion batteries (LIBs) have achieved tremendous success as power sources in various portable electronic devices and electric vehicles (EVs) especially in recent years, because of their appealing properties such as long cycle life, high working voltage, and high capacity and energy.[1] However, the availability of lithium resources in India is questionable and the world-wide availability of lithium resources is also debatably insufficient to offer cost effective storage solutions to this modern energy era. Towards this direction, sodium-ion batteries (SIBs) offer convincing advantages in terms of the abundant availability of sodium, apart from being eco-benign and having easy processing protocols, due to which they have recently attracted a great deal of interest for large scale energy storage applications.[2] Sodium, being the 4th most abundant element available to the extent of 2.64 wt% on the earth leaves behind ample scope to exploit it as an alternative counterpart in the rechargeable cell assembly to realize sodium-ion batteries, similar to those of lithium-ion batteries and hence SIBs receive prime focus as sustainable energy devices for the next generation.[3]

Actually, most of the SIB research is devoted on the exploration of stable and low-cost positive electrode materials, including $NaCoO_2$, $Na_{0.44}MnO_2$, $NaTi_2(PO_4)_3$, $Na_3V_2(PO_4)_3$ and $NaNi_{0.5}Mn_{0.5}O_2$.[4–10] On the other hand, only few reports are available on the anode materials of SIBs involving hard carbon, red phosphorus, $Na_2Ti_3O_7$, SnS, MoS_2, Sn_4P_3 and SnSb.[11–18] Stevens and Dahn *et al.*, reported that hard carbon is the top ranked non graphitic carbonaceous material suitable for sodium storage, due to the large interlayer distance and the disordered structure.[12] However, some disadvantages are reported for non-graphitic carbonaceous materials such as larger irreversible capacity and poor capacity retention.[11,12,19,20] To the interest of any researcher, graphite, the commonly used commercial electrode for LIBs due to its proven stable capacity obviously becomes the first choice of anode to be explored for other energy storage devices also. However, graphite does not function as a potential anode in SIBs, due to the inherent difficulties involved in the insertion of sodium ions based on size factor. *i.e.* insertion of Na^+ ions into graphite is severely limited, because of its larger radius (0.95 Å) compared with that of Li ion (0.6 Å). As a result, significantly lesser reversible capacity could be extracted from graphite in SIBs cell assembly in comparison with LIBs. Such a critical issue indicates the pressing need to identify and to develop alternative anode materials for SIBs, which in turn is expected to exhibit high specific capacity, long cycle life, desirable rate capability and to ensure environmentally benign nature in order to meet with the

CSIR-Central Electrochemical Research Institute, Karaikudi-630 006, Tamilnadu, India. E-mail: kalaiselvicecri@gmail.com; Tel: +91 4565 241427

† Electronic supplementary information (ESI) available. See DOI: 10.1039/c7ra02289a

requirements of safer and potential energy storage applications. In this regard, Na-alloying metals based on Sn and Sb have been investigated as anode materials for SIBs, based on the fact that they are bestowed with high Na storage capacity. Xiao *et al.*, reported that SnSb/C nanocomposite exhibits a capacity of 274 mA h g^{-1} at 1000 mA g^{-1}.[18] But, this alloy anode suffers from huge volume changes upon charging/discharging, which is a serious and hampering issue against its global acceptance.

Alternatively, transition-metal oxides (conversion anode materials), recommended as promising candidates for LIBs, owing to their high theoretical capacity with superior lithium storage properties and natural abundance triggers unassuming interest to exploit them in SIBs also. In this regard, simple metal oxides such as MoO_3, TiO_2, Fe_3O_4, *etc.* have been used as anode material for SIBs.[21–23] Balaya group demonstrated that MoO_3 anode exhibits higher discharge/charge capacity of 771 and 410 mA h g^{-1} during the first cycle and an acceptable progressive capacity of 130 mA h g^{-1} up to 500 cycles.[21] Recently, Chen *et al.*, reported that graphene coupled TiO_2 anode delivers a capacity of 90 mA h g^{-1} at a high rate of 1.2 A g^{-1} and its cycleability up to 4000 cycles has also been demonstrated.[22] According to Komaba *et al.*, nanostructured Fe_3O_4 anode delivers a capacity of 160 mA h g^{-1}.[23] Despite the availability of such encouraging reports, one cannot ignore the fact that all such simple transition metal oxides invariably suffer from volume expansion problem, especially during repeated charging/discharging process, which in turn leads to the deterioration of electrode and an unavoidable or unacceptable capacity fade in rechargeable cell assembly, may it be LIBs or SIBs. As an alternative measure to the obvious choice of simple transition metal oxides, binary or multi metal oxides exhibit higher electrical conductivity and lager specific capacity, determined solely by the select chemical composition and the synergistic effect of the metals involved. In this connection, Tirado *et al.*, in as early as 2002 have investigated and reported that the spinel $NiCo_2O_4$ compound could be deployed as anode for SIBs, which delivers a reversible capacity of 200 mA h g^{-1}.[24] However, no further reports about these spinel family electrodes for SIBs are available up to this time for reasons unknown.

Actually, binary or ternary transition metal oxides also pose volume expansion and contraction related problems associated with sodiation and desodiation, but the advantage of mutual combating of shortcomings by each metal will offset the severity of the issue to a greater extent. Based on these reasons, cost effective and eco-benign metal oxide composition, *viz.*, $ZnMn_2O_4$ (ZMO) has been chosen and to avoid the fear for volume expansion related capacity fade behaviour, decoration of nanoparticles of ZMO with a carefully chosen compatible carbon matrix has been aimed through the present study. In this connection, nitrogen doped graphene (NG) has been selected to prepare the composite of ZMO, because of its superior conductivity, layered sheet like morphology, larger surface area and excellent mechanical flexibility.

In other words, with an objective of preventing the volume expansion and to restrain the aggregation of ZMO nanoparticles during charge and discharge process, composite of ZMO prepared with nitrogen doped graphene by simple sonication method has been investigated and validated as an alternative anode material for SIBs. When evaluated for its anode behaviour, ZMO/NG composite exhibits an apparent capacity of 170 mA h g^{-1} and appreciable cycling behaviour compared with pristine ZMO anode in SIBs. To the best of our knowledge, there is no report available on ZMO as anode for SIBs and hence the present communication is the ever first report on ZMO anode, requiring no comparison of performance in SIBs.

Basically, ZMO nanoparticles were synthesized at an optimum pH value of 11, maintained in the precursor solution and subjected further to hydrothermal treatment to obtain flakes, composed of interconnected nanoparticles. Such flakes upon sonication with NG leads to the dispersion of ZMO nanoparticles on the sheets of NG, which upon thermal treatment gets distributed uniformly.

2. Experimental section

2.1 Synthesis of $ZnMn_2O_4$ nanoflakes

Deionized (DI) water has been used throughout the experiment and the chemicals were used as received without further purification. ZMO flakes have been prepared as follows: 1 mmol zinc nitrate hexahydrate ($Zn(NO_3)_2 \cdot 6H_2O$) and 2 mmol manganese(II) nitrate hydrate ($Mn(NO_3)_2 \cdot xH_2O$) (Alfa Aesar) were dissolved in 35 mL deionized water, followed by the addition of 0.075 g glycine and 0.142 g Na_2SO_4 salt. The reactants were dissolved in distilled water with magnetic stirring to get a homogeneous solution. For the above solution, the pH was fixed at 11 by the dropwise addition of 5 M NaOH solution and stirred for 1 h. The obtained solution was transferred into 50 mL Teflon-lined stainless steel autoclave and heated at 180 °C for 20 h. Subsequently, the autoclave was cooled to room temperature and the dense white colour precipitate was washed with distilled water and with acetone several times, and dried at 70 °C for 10 h in vacuum. Finally, the dried powder was calcined at 600 °C for 2 h with a heating rate 2 °C min^{-1} to obtain ZMO flakes.

2.2 Preparation of $ZnMn_2O_4$/NG composite

ZMO/NG nanocomposite was prepared by mixing the as-prepared ZMO flakes with the commercial grade nitrogen doped graphene (10 wt%) in ethanol and sonicated for 60 minutes. Such a sonication will lead to the disintegration of nanoflakes in to nanoparticles and thus paves way to get a homogenous mixing of ZMO nanoparticles with those of NG. The resultant mixture was dried in oven at 60 °C overnight, and the contents were heated in the furnace at 400 °C for 2 h in Ar atmosphere to get better wrapping of ZMO with due adherence by the added NG powder. The resulting material is denoted as ZMO/NG nanocomposite. Nanocrystalline particles of ZMO obtained through sonication of ZMO flakes has been considered as pristine ZMO for physical and electrochemical characterization to compare the performance characteristics with that of subsequently prepared ZMO/NG nanocomposite.

2.3 Physical characterization

The crystal structure of the material was characterized by Bruker D8 Advance X-ray diffractometer using Ni-filtered Cu Kα

radiation (λ = 1.5406 Å). To study the particle size, surface morphology and structure of the sample, scanning electron microscopy (SEM, JEOL JSM6480LV system) and transmission electron microscopy (TEM, Tecnai 20 G2 (FEI make)) were used.

2.4 Electrochemical characterization

Electrochemical measurements were carried out using CR2032 type coin cells, wherein copper foil has been used as the current collector and sodium metal as counter and reference electrode. A solution consisting of 1.0 M $NaClO_4$ dissolved in 1 : 1 (v/v) mixture of ethylene carbonate (EC)/dimethyl carbonate (DMC) serves as the electrolyte. The working electrode was prepared by mixing ZMO/NG (70 wt%) as the active material, conductive carbon (Super-P) (20 wt%) and polyvinylidene fluoride binder (10 wt%) using *N*-methyl-2-pyrrolidone as solvent. The mixture was made as slurry and coated on copper foil. The coated electrode was dried in oven at 80 °C to evaporate NMP, hot roll pressed to ensure better adherence and cut in to circular discs of 15.5 mm diameter to act as anode in the coin cell assembly. Cyclic Voltammetry (CV) was recorded with VMP3 multichannel potentiostat–galvanostat system (Biologic Science Instrument) in the potential window of 0.01–3.0 V and at the scan rate of 0.1 mV s^{-1}. The charge–discharge behaviour was investigated with Arbin battery cycler. Electrochemical impedance spectroscopy (EIS) measurements were carried out on a Biologic VSP electrochemical work station in the frequency ranging from 10 kHz to 100 mHz with an amplitude voltage of 10 mV at room temperature.

3. Results and discussion

Since the details of physical characterization have already been reported,[25] the current communication deals with the results of electrochemical characterization related to the application of ZMO/NG as an anode for SIBs. To investigate the effect of NG on ZMO with respect to Na-ion insertion/extraction behaviour, we have carried out the electrochemical characterization such as cyclic voltammetry (CV) and galvanostatic discharge/charge cycling studies with respect to bare ZMO and ZMO/NG nanocomposite anodes individually. Fig. 1a and b shows the first three cycle behaviour cyclic voltammetry curves of the as-prepared pristine ZMO and ZMO/NG composite electrodes recorded individually at a scan rate of 0.1 mV s^{-1} in the voltage range of 0.01 to 3.0 V *versus* Na^+/Na. The first cycle CV behaviour of ZMO and ZMO/NG composite anode exhibits a peak around 1.1 V, which is due to the reduction of Mn^{3+} to Mn^{2+}. Followed by this, another peak that appears around 0.9 V is due to the formation of solid electrolyte interphase (SEI).[26] Consequent to these two peaks, yet another high intensity peak around 0.2 V is seen, owing to the reduction of Mn^{2+} and Zn^{2+} to their respective metallic nanodomains of Mn^0 and Zn^0. In the anodic process, peaks corresponding to the oxidation of Mn^0 to Mn^{2+} and Zn^0 to Zn^{2+} appear at 0.8 and 2.1 V along with the decomposition of Na_2O matrix.[27,28] In the subsequent cathodic scans, peaks at 1.1 and 0.9 V disappear due to the direct reduction of Mn^{2+} to Mn^0 and also due to the fact that a stable SEI film is formed during the 2nd cycle and gets maintained thereafter, which is noteworthy.

Herein, ZMO/NG nanocomposite anode, especially from second cycle onwards exhibits perfect overlapping behaviour of CV peaks, which is more significant than the one observed with pristine ZMO anode (peak intensity and integral area decrease upon cycling). This in turn is an evidence that the sodium insertion and extraction reaction of ZMO/NG nanocomposite anode takes place much readily and attributes to the excellent reversibility behaviour in SIBs.

Fig. 2a illustrates the charge/discharge performance of ZMO/NG and ZMO anodes under a current density of 100 mA g^{-1}. The first discharge and charge capacity values of bare ZMO anode are 210 and 80 mA h g^{-1} respectively and the coulombic efficiency is 38% (Fig. 2a). On the other hand, ZMO/NG nanocomposite exhibits a very high initial discharge capacity of 1025 mA h g^{-1} and a nominal charge capacity of 410 mA h g^{-1}, corresponding to an inferior coulombic efficiency of 40%, which is however slightly higher than that of pristine ZMO anode. Interestingly, the composite ZMO/NG anode delivers a progressive capacity of 170 mA h g^{-1} up to 1000 cycles, without any significant capacity decay, due to the presence of NG that facilitates the facile and sustainable sodium transport across the interface *via* effective mitigation of volume changes upon repeated cycling. In contrast, the charge/discharge behaviour of pristine ZMO anode exhibits a drastic decrease in capacity (50 mA h g^{-1} after 150 cycles (Fig. 2a)) compared with that of ZMO/NG composite under the influence of 100 mA g^{-1} current density and the same could be attributed to the inferior conductivity and the uncontrollable volume changes that occur during cycling. The superior sodium storage performance of

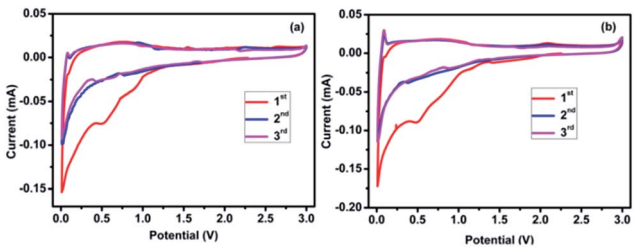

Fig. 1 Cyclic voltammogram of (a) pristine ZMO and (b) ZMO/NG composite anode recorded at a scan rate of 0.1 mV s^{-1} in the range of 0.01–3.0 V *versus* Na^+/Na.

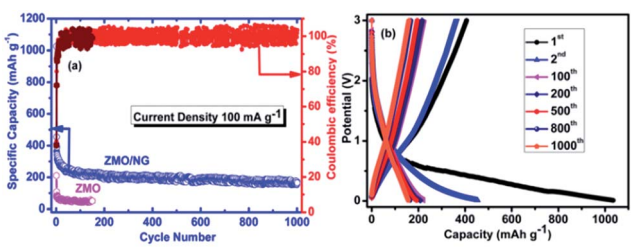

Fig. 2 (a) Cycling performance of the ZMO/NG and ZMO electrodes at 100 mA g^{-1} and (b) charge–discharge profile of ZMO/NG electrode at 100 mA g^{-1} for 1000 cycles.

ZMO/NG is due to the synergistic effect of presence and distribution of ZMO nanoparticles which are widely decorated on the NG sheets, which in turn can effectively accommodate sodium as well as offer the required cushioning effect against the strain caused due to repeated charge/discharge process.

In order to investigate the effect of NG in alleviating and accommodating the volume expansion/contraction of ZMO present in ZMO/NG composite anode during sodiation and desodiation, post cycling TEM and SEM analysis have been carried out. Fig. 3 and S1† display TEM and SEM images of bare ZMO and ZMO/NG composite electrodes after completing 150 and 1000 cycles, respectively. After 150 cycles itself, pristine ZMO nanoparticles exhibit visible change in their size and the resultant presence of agglomerated particles is obvious from Fig. 3a and b. On the other hand, Fig. 3c and d are TEM images of ZMO/NG after 1000 cycles, wherein presence of individual particles entrapped by graphene sheet and the absence of agglomeration or change in the particle size are evident. Similarly, Fig. S1† displays the SEM images of both ZMO (Fig. S1a and b†) and ZMO/NG anode (Fig. S1c and d†), evidencing the presence of SEI layer that gets maintained to facilitate reversible sodiation/desodiation even after completing 150 and 1000 cycles respectively. All the observed results reveal the importance of flexible NG sheets present in ZMO/NG composite and its role in preventing the structure collapse and pulverization caused generally by volume expansion, apart from providing a facile conductive path to enhance capacity during extended charge/discharge cycles.

Fig. 2b shows the charge/discharge profile of 1st, 2nd, 100th, 200th, 500th and 1000th cycle of ZMO/NG nanocomposite anode recorded at a current density of 100 mA g^{-1} in the potential range of 0.01–3.0 V. The first discharge curve shows a plateau from 1.1 to 0.5 V which is due to the reduction of Mn^{3+} to Mn^{2+} and SEI, respectively. Followed by this, a small plateau at 0.2 V is seen and is attributed to the reduction of Zn^{2+} and Mn^{2+} to the respective metallic nanodomains of Zn^0 and Mn^0 (eqn (1)). In particular, during the first anodic sweep, plateau found at 0.8 V could be attributed to the oxidation of Mn^0 to Mn^{2+} and Zn^0 to Zn^{2+} (eqn (2) and (3)). These plateaus are matching well with the CV results. Since there are few contradictory reports available about the mechanism of transition metal oxides used in SIBs.[24] XRD analysis (Fig. S2†) was done for ZMO/NG composite after completing 1000 cycles with a view to gain more understanding on the same. Presence of characteristic Mn_xO_y and Zn_xO_y peaks observed in the post cycling XRD pattern confirms the involvement of conversion mechanism and the resultant formation of ZnO and MnO upon sodiation/desodiation process. Hence it is understood that ZMO anode follows similar conversion mechanism in SIBs as that of LIBs. Accordingly, the following mechanism stands valid for the present study.

$$ZnMn_2O_4 + 8Na^+ + 8e^- \rightarrow Zn + 2Mn + 4Na_2O \quad (1)$$

$$2Mn + 2Na_2O \leftrightarrow 2MnO + 4Na^+ + 2e^- \quad (2)$$

$$Zn + Na_2O \leftrightarrow ZnO + 2Na^+ + 2e^- \quad (3)$$

In addition to the long cycling stability and excellent capacity retention, ZMO/NG anode displays high rate capability also (Fig. 4). ZMO/NG nanocomposite anode examined under different current density conditions, *viz.* 50, 100, 400, 500, 1000, 2000, 5000 and 10 000 mA g^{-1} delivers specific capacity values of 425, 245, 180, 140, 90, 70, 33 and 15 mA h g^{-1}, respectively. After high rate cycling at 10 A g^{-1} condition, when the cell is switched back to the initial 50 mA g^{-1} condition, ZMO/NG anode still delivers an appreciable capacity of 290 mA h g^{-1} up to 150 cycles, which is noteworthy. This high rate performance of ZMO/NG nanocomposite anode is attributed to the twin advantages derived from NG that includes the presence of ZMO nanoparticles decorated on the surface of NG which enhances the Na-ion transport kinetics and the ability of NG in tolerating the expansion and contraction of ZMO as a buffering agent.

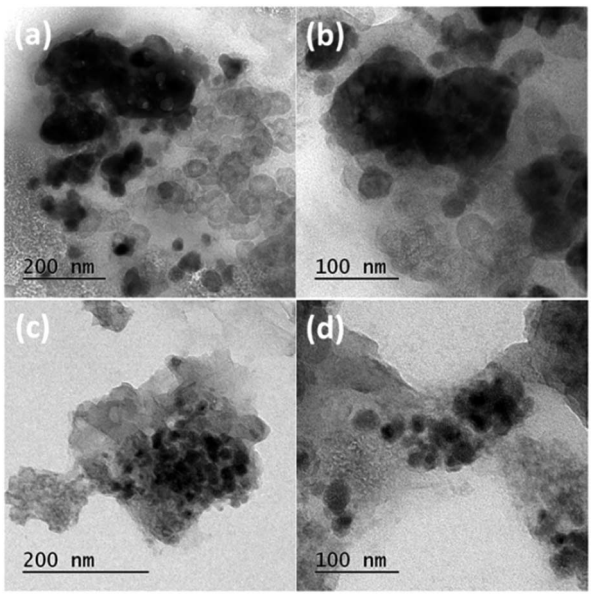

Fig. 3 Post cycling TEM images of (a and b) ZMO after 150 cycles and (c and d) ZMO/NG nanocomposite electrode after 1000 charge/discharge cycles at a current density of 100 mA g^{-1}.

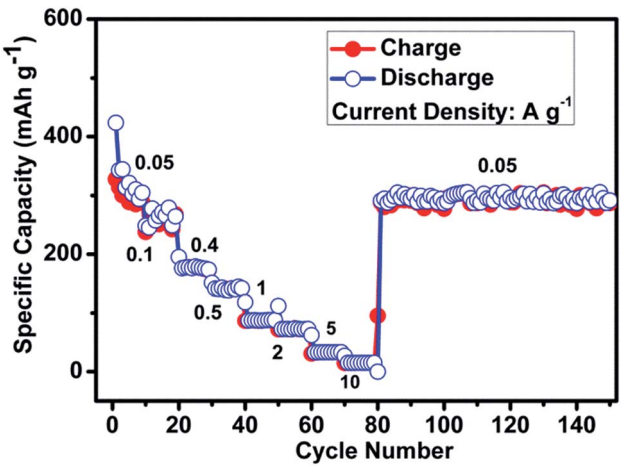

Fig. 4 Rate capability of ZMO/NG nanocomposite anode under the influence of different current density conditions.

To gain further detailed Na-ion storage performance in terms of reaction kinetics of ZMO/NG nanocomposite anode, we have carried out electrochemical impedance spectroscopy (EIS) measurements in the frequency range of 10 kHz to 100 mHz, for conditions such as before and after cycling and the results are appended in Fig. S3.† ZMO/NG nanocomposite anode exhibits significantly lower charge transfer resistance even after completing 1000 cycles compared with the as fabricated electrode, thus demonstrating the mechanical stability and superior electrochemical performance of the composite electrode. These results demonstrate that presence of nanoparticles of ZMO plays an important role in enhancing the reaction kinetics by way of reducing the Na^+ diffusion rate and the beneficial role of NG in improving the electronic conductivity and towards the mitigation of volume changes upon extended cycles.

4. Conclusions

We synthesized a ZMO/NG nanocomposite *via* simple sonication, consisting of hydrothermally prepared $ZnMn_2O_4$ flakes, composed of nanoparticles along with nitrogen doped graphene and the resultant composite has been exploited as anode material for sodium ion batteries for the first time. The composite electrode material exhibits excellent electrochemical performance in terms of long cycle life (1000 cycles) and high rate capability (10 A g^{-1} condition). In particular, the custom synthesized ZMO/NG composite anode exhibits a steady state capacity of 170 mA h g^{-1} for 1000 cycles at 100 mA g^{-1} condition. Further, ZMO/NG nanocomposite anode possesses excellent tolerance and appreciable stability up to 10 A g^{-1} condition. This communication clearly indicates that ZMO/NG composite anode could be recommended as an alternative and potential anode material for sodium ion batteries.

Acknowledgements

Financial support from University Grants Commission for the UGC-Senior Research Fellowship and Council of Scientific and Industrial Research (CSIR) through MULTIFUN program is gratefully acknowledged.

Notes and references

1 G. Bruce, B. Scrosati and J. M. Tarascon, *Angew. Chem., Int. Ed.*, 2008, **47**, 2930–2946.
2 Y. Sun, L. Zhao, H. Pan, X. Lu, L. Gu, Y.-S. Hu, H. Li, M. Armand, Y. Ikuhara, L. Chen and X. Huang, *Nat. Commun.*, 2013, **4**, 1870–1879.
3 Y. Jiang, M. Hu, D. Zhang, T. Yuan, W. Sun, B. Xu and M. Yan, *Nano Energy*, 2014, **5**, 60–66.
4 C. Delmas, J. J. Braconnie, C. Fouassier and P. Hagenmuller, *Solid State Ionics*, 1981, **4**, 165–169.
5 R. Berthelot, D. Carlier and C. Delmas, *Nat. Mater.*, 2011, **10**, 74–80.
6 F. Sauvage, L. Laffont, J. M. Tarascon and E. Baudrin, *Inorg. Chem.*, 2007, **46**, 3289–3294.
7 X. Li, X. Zhu, J. Liang, Z. Hou, Y. Wang, N. Lin, Y. Zhu and Y. Qian, *J. Electrochem. Soc.*, 2014, **161**, A1181–A1187.
8 Z. Jian, L. Zhao, H. Pan, Y.-S. Hu, H. Li, W. Chen and L. Chen, *Electrochem. Commun.*, 2012, **14**, 86–89.
9 Y. H. Lu, L. Wang, J. G. Cheng and J. B. Goodenough, *Chem. Commun.*, 2012, **48**, 6544–6546.
10 S. M. Oh, S. T. Myung, J. Hassoun, B. Scrosati and Y. K. Sun, *Electrochem. Commun.*, 2012, **22**, 149–152.
11 S. Komaba, W. Murata, T. Ishikawa, N. Yabuuchi, T. Ozeki, T. Nakayama, A. Ogata, K. Gotoh and K. Fujiwara, *Adv. Funct. Mater.*, 2011, **21**, 3859–3867.
12 D. A. Stevens and J. R. Dahn, *J. Electrochem. Soc.*, 2000, **147**, 1271–1273.
13 M. Dahbi, N. Yabuuchi, K. Kubota, K. Tokiwa and S. Komaba, *Phys. Chem. Chem. Phys.*, 2014, **16**, 15007–15028.
14 A. Rudola, K. Saravanan, C. W. Masona and P. Balaya, *J. Mater. Chem. A*, 2013, **1**, 2653–2662.
15 T. F. Zhou, W. K. Pang, C. F. Zhang, J. P. Yang, Z. X. Chen, H. K. Liu and Z. P. Guo, *ACS Nano*, 2014, **8**, 8323–8333.
16 K. Chang and W. X. Chen, *ACS Nano*, 2011, **5**, 4720–4728.
17 J. Qian, Y. Xiong, Y. Cao, X. Ai and H. Yang, *Nano Lett.*, 2014, **14**, 1865–1869.
18 L. F. Xiao, Y. L. Cao, J. Xiao, W. Wang, L. Kovarik, Z. M. Nie and J. Liu, *Chem. Commun.*, 2012, **48**, 3321–3323.
19 K. Tang, L. J. Fu, R. J. White, L. H. Yu, M. M. Titirici, M. Antonietti and J. Maier, *Adv. Energy Mater.*, 2012, **2**, 873–877.
20 Y. Cao, L. Xiao, M. L. Sushko, W. Wang, B. Schwenzer, J. Xiao, Z. Nie, L. V. Saraf, Z. Yang and J. Liu, *Nano Lett.*, 2012, **12**, 3783–3787.
21 S. Hariharan, K. Saravanan and P. Balaya, *Electrochem. Commun.*, 2013, **31**, 5–9.
22 C. Chen, Y. Wen, X. Hu, X. Ji, M. Yan, L. Mai, P. Hu, B. Shan and Y. Huang, *Nat. Commun.*, 2015, **6**, 6929–6937.
23 S. Komaba, T. Mikumo, N. Yabuuchi, A. Ogata, H. Yoshida and Y. Yamada, *J. Electrochem. Soc.*, 2010, **157**, A60–A65.
24 R. Alcantara, M. Jaraba, P. Lavela and J. L. Tirado, *Chem. Mater.*, 2002, **14**, 2847–2848.
25 B. Chandra Sekhar, P. Packiyalakshmi and N. Kalaiselvi, *ChemElectroChem*, DOI: 10.1002/celc.201600914.
26 Y. Liu, N. Zhang, C. Yu, L. Jiao and J. Chen, *Nano Lett.*, 2016, **16**, 3321–3328.
27 X. H. Wu, W. W. Wu, K. T. Wang, W. Chen and D. He, *Mater. Lett.*, 2015, **147**, 85–87.
28 J. Chen, Q. Ru, Y. Mo, S. Hu and X. Hou, *Phys. Chem. Chem. Phys.*, 2016, **18**, 18949–18957.